Solar-Terrestrial Physics. 2023. Vol. 9. Iss. 3. P. 86–92. DOI: 10.12737/stp-93202310. © 2023 N.M. Gavrilov, S.P. Kshevetskii. Published by INFRA-M Academic Publishing House

UDC551.511.31
DOI: 10.12737/stp-93202310

Received February 19, 2023
Accepted May 10, 2023

IDENTIFICATION OF SPECTRUM OF SECONDARY ACOUSTIC-GRAVITY WAVES IN THE MIDDLE AND UPPER ATMOSPHERE IN A HIGH-RESOLUTION NUMERICAL MODEL

N.M. Gavrilov
Saint-Petersburg State University,
Saint Petersburg, Russia, n.gavrilov@spbu.ru

S.P. Kshevetskii
I. Kant Baltic Federal University,
Kaliningrad, Russia, renger@mail.ru
A.M. Obukhov Institute of Atmospheric Physics RAS,
Moscow, Russia

Abstract. Considerable attention has recently been paid to the study of so-called "secondary" acoustic-gravity waves (AGWs) that arise as a result of instability and nonlinear interactions of "primary" wave modes propagating from atmospheric sources, among themselves, and with the mean flow. In this paper, for the first time, the horizontal spatial spectra of primary and secondary AGWs are separated at fixed altitude levels in the middle and upper atmosphere at different time moments, which are simulated using a three-dimensional nonlinear high-resolution model AtmoSym. It is shown that in a short time after switching on the plane wave source at the lower boundary of the model, the spectrum consists of a peak corresponding to primary AGW and quasi-white noise generated by random atmospheric disturbances and the numerical model. Later, secondary peaks appear in the spectra at horizontal wave numbers, which are multiples of the wave numbers of primary AGW. The proposed separation of the spectra of primary and secondary AGWs makes it possible to estimate the relative contribution of secondary AGW at different altitudes, at different times, and with different stability of background temperature and wind profiles in the atmosphere.

Keywords: acoustic-gravity waves, spectrum, secondary waves, numerical simulation, upper atmosphere, middle atmosphere.

INTRODUCTION

Acoustic-gravity waves (AGWs) play an important role in the dynamics of the middle and upper atmospheric layers. AGWs generated in the lower atmosphere propagate upward into the mesosphere and thermosphere, transferring momentum and energy to higher layers of the atmosphere. Due to dissipation and momentum transfer to the mean flow, they can cause the zonal circulation to turn in the mesosphere/lower thermosphere and affect the general circulation of the middle and upper atmosphere. Studies [Yigit, Medvedev, 2009; Yigit et al., 2009; Miyoshi et al., 2014] have shown that the mean-flow wave accelerations caused by dissipation of AGWs coming from the troposphere play an important role in maintaining the momentum balance in the thermosphere. Thus, to understand the dynamics of the atmosphere as a whole and its layers requires adequate knowledge of AGWs.

To take into account AGW effects in global circulation models, mesoscale waves and their interaction with the mean flow should be parameterized, and these parameterizations should be compared with experimental data [Alexander et al., 2010; Geller at al., 2013]. Nowadays, high-resolution numerical models of global circulation [Miyoshi, Fujiwara, 2008; Becker et al., 2015] can firstly simulate only large-scale AGWs and secondly are relatively expensive. That is why there is still a need for effective parameterizations of thermal and dynamic AGW effects for climate models or complex models of the atmosphere–ionosphere system. There are a number of such parametrizations, with AGW sources being also parametrized or being specified from observations or climatological studies of AGWs in the lower atmosphere.

Numerical simulation of nonlinear small-scale waves and turbulence in the atmosphere has been rapidly developing in recent years. Fritts et al. [2009, 2014] have simulated the breaking of atmospheric internal waves and Kelvin—Helmholtz instabilities. Their models are three-dimensional and describe propagation and breaking of AGWs in rectangular atmospheric regions with limited horizontal and vertical dimensions. Two-dimensional numerical models of atmospheric AGWs have been developed by Yu et al. [2009] and Liu et al. [2008]. A two-dimensional version of the ICON model is currently used at the Institute of Atmospheric Physics (Kuhlungsborn, Germany) [Gassmann, Herzog, 2015].

Gavrilov and Kshevetskii [2014] have developed a high-resolution three-dimensional numerical model describing propagation of nonlinear AGWs through the atmosphere from the Earth surface to the thermosphere. The numerical scheme adequately takes into account the fundamental laws of conservation of mass, momentum, and energy, as well as the law of non-decreasing entropy. This model can provide physically correct generalized solutions of hydrodynamic equations, as well as can ensure the stability of the numerical scheme in the field of breaking of nonlinear waves and transition to

turbulence, where many computational algorithms become invalid. With the wide range of heights under study, this stable algorithm makes the numerical model suitable for simulating AGWs and their instability at heights from the Earth surface to the thermosphere. Numerical simulation provides further insight into the mechanisms of dynamic interaction between different atmospheric layers.

When AGWs break down in the middle and upper atmosphere, strong nonlinearity and cascaded energy transfer to smaller-scale waves occur. Small-scale secondary wave modes of AGWs are shorter than primary breaking AGWs. These secondary AGWs can boost the transition of wave energy to turbulence, and can also produce significant wave fluxes of momentum. Moreover, secondary AGWs can cause inhomogeneities of background fields with dimensions comparable to horizontal dimensions of wave packets [Vadas, Fritts, 2002]. These inhomogeneities can, in turn, excite secondary wave modes with horizontal lengths greater than those of primary waves. The long secondary waves have high horizontal phase velocities and long vertical lengths. They can transfer energy and momentum more effectively and propagate to higher altitudes in the upper atmosphere.

The primary AGWs that propagate from the troposphere can create localized regions of increased and decreased momentum and energy fluxes in the middle and upper atmosphere [Fritts et al., 2006; Smith et al., 2016]. Irregularities of the related wave accelerations can lead to generation of upward and downward secondary AGWs with horizontal lengths of the order of scales of the irregularities. Secondary AGWs can also be generated when primary AGWs are broken down, accompanied by strong nonlinearity. Such secondary AGWs arise as high harmonics and usually have lengths and periods shorter than primary wave modes [Bacmeister, Schoeberl, 1989; Franke, Robinson, 1999]. Since the first mechanism produces longer secondary waves with higher phase velocities, they can propagate to higher altitudes. Intense secondary waves can, in turn, break down and cause additional accelerations at high altitudes.

Simulation has shown that the primary AGWs excited by deep convection can reach the thermosphere, where they break down and dissipate [Vadas, Liu, 2013; Vadas, Crowley, 2010]. This process causes irregular localized accelerations, which excite secondary AGWs with long lengths [Vadas, Crowley, 2010]. Such secondary AGWs can then propagate up to much higher altitudes, leading to considerable variability in the neutral wind [Vadas, Crowley, 2017]. Furthermore, these secondary AGWs increase the variability of the ionosphere by generating medium- and large-scale traveling ionospheric disturbances [Azeem et al., 2017; Vadas, Crowley, 2017]. Recent experimental data suggest that secondary AGWs can be formed in the winter polar stratosphere and then can be observed in the mesosphere and lower thermosphere [Chen et al., 2016; Zhao et al., 2017].

Analysis of literature sources shows that generation of secondary AGWs is an important process that strongly modifies the wave energy and momentum transfer and transformation mechanisms. A more detailed study of secondary AGWs requires developing high-resolution numerical models and methods for separating the spectra of primary and secondary wave modes.

This article describes the formulation of the problem of simulating plane waves in the high-resolution model AtmoSym and an algorithm that allows us to separate spectra of primary AGWs, generated by a wave source at the lower boundary of the model, and secondary AGWs, produced by these primary waves in different layers of the middle and upper atmosphere. Examples are given which illustrate the gradual formation of the spectrum of secondary waves after switching on the wave source in the model.

1. NUMERICAL MODEL

We have used AtmoSym, a high-resolution three-dimensional numerical model developed by Gavrilov and Kshevetskii [2014], which is available online for free [http://atm os.kantiana.ru/language/ru]. The model is based on the plane geometry and complete hydrodynamic three-dimensional equations [Gavrilov, Kshevetskii, 2014]. AtmoSym takes into account dissipative and nonlinear processes affecting AGW propagation, and can describe such complex processes as instability of AGWs, their breaking, and turbulence generation.

Background temperature profiles $T_0(z)$ for the simulation have been taken from the semi-empirical atmospheric model NRLMSISE-00 [Picone et al., 2002]. Background dynamic coefficients of dynamic molecular viscosity and thermal conductivity are estimated using Sutherland's formula [Kikoin, 1976]. The AtmoSym model also includes background turbulent viscosity and thermal conductivity that reach maxima of ~10 m^2/s in the boundary layer and the lower thermosphere and a minimum of 0.1 m^2/s in the stratosphere [Gavrilov, Kshevetskii, 2014]. Zero values of vertical temperature gradients and horizontal velocity, as well as zero vertical velocity are set at the upper boundary [Gavrilov, Kshevetskii, 2014]. Under such upper boundary conditions, the AGWs coming from the underlying layers of the atmosphere may be reflected. The upper boundary in this study is set at an altitude of 600 km, where molecular viscosity and thermal conductivity are very high, and the reflected waves are subject to strong attenuation. Numerical tests indicate that the influence of upper boundary conditions is negligible at distances from the upper boundary that are twice the height of a homogeneous atmosphere. Thus, at altitudes to 200 km we analyze, the influence of upper boundary conditions is insignificant. The lower boundary conditions on the Earth surface have the following form (see [Gavrilov, Kshevetskii, 2014]):

$$\begin{aligned} &(T')_{z=0} = 0,\ (u)_{z=0} = 0,\ (v)_{z=0} = 0, \\ &(w)_{z=0} = W_0 \cos\left(\sigma t - \vec{k}_h\, \vec{r}\right), \end{aligned} \qquad (1)$$

where T', u, v, w are wave disturbances of temperature and velocity components along the horizontal X, Y axes and the vertical Z-axis respectively. The latter relation for the vertical velocity on the Earth surface in (1) serves as a source of plane AGWs in the AtmoSym model, where W_0 and σ are the amplitude and frequency of wave excitation; $\vec{k_h}\left(k_x, k_y\right)$ and $\vec{r_h}\left(x, y\right)$ are the horizontal wave vector and the radius vector, and k_x and k_y are the wave numbers along the horizontal X and Y axes. The plane wave modes can be considered as spectral components of tropospheric convective, turbulent, and meteorological processes. These processes can be parametrized by corresponding sets of effective spectral components of vertical velocity at the lower boundary of the atmosphere [Townsend, 1965, 1966]. Along the horizontal X and Y axes, we can assume a periodicity of wave fields.

Numerical simulation begins in windless conditions of the undisturbed atmosphere with vertical profiles of background temperature, density, molecular weight, and molecular kinematic viscosity corresponding to January at 50° N under moderate solar activity according to the NRLMSISE-00 model [Picone et al., 2002]. Previous studies using the AtmoSym model have shown that a sharp activation of surface wave source (1) can give rise to an intense initial AGW impulse, which can reach high altitudes in a few minutes. To slow down the rate of the wave source activation, we multiply the vertical velocity amplitude at lower boundary (1) by a Gaussian function increasing from zero at t=0 to 1 at t=t_a (for more detail, see [Gavrilov et al., 2022]). The moment t_a is considered the time of wave source activation in the model; and at t>t_a, the amplitude of the source W_0 in (1) does not change.

At low amplitudes of the wave source in (1), the numerical solution in the lower and middle atmosphere should be expected to tend at $t \gg t_a$ to steady-state plane AGWs corresponding to the standard linear theory (e.g., [Gossard, Hooke, 1975]). Gavrilov et al. [2015] have revealed a close correlation between the simulated amplitudes of different wave fields and the polarization relations of the linear theory of AGWs [Gossard, Hooke, 1975] at $t \gg t_a$ at altitudes to 100 km.

2. IDENTIFICATION OF SPECTRUM OF SECONDARY AGWs

In this paper as in Gavrilov et al. [2022], we examine AGW modes propagating along the eastward X-axis and assume that the horizontal dimension of the atmospheric region under study is equal to the length of the latitude circle at 50° N, L_h≈27 000 km. At the horizontal boundaries of this latitude circle, we apply periodic boundary conditions (see [Gavrilov, Kshevetskii, 2014]). The simulation has been carried out using wave source (1) with AGW amplitudes within W_0=0.01–0.1 mm/s. The lowest amplitudes correspond to weak AGWs, for which the nonlinear effects are small at all the heights considered. At W_0~0.1 mm/s, intense AGWs are excited which are subject to significant nonlinear interactions in the mesosphere and lower thermosphere.

The range of horizontal phase velocities c_h~50–200 m/s we use is peculiar to AGWs with relatively long vertical wavelengths, which can propagate from the Earth surface to the upper atmosphere. The number of wavelengths along the latitude circle n=32, which corresponds to the horizontal wavelength λ_h=L_h/n≈840 km and the AGW periods τ=λ_h/c_h~4.7–1.2 hr for the above range of c_h values. The step between nodes of the horizontal grid of the numerical model Δx=λ_h/16; and the time step of calculations Δt≈2.9 s. The vertical grid of the model covers heights from the Earth surface to 600 km and contains 1024 unequally spaced nodes. The step of the vertical grid varies from 12 m at the bottom to 3 km near the upper boundary, so about 70 % of the grid nodes are located in the lower and middle atmosphere.

The spatial spectra of the simulated hydrodynamic fields by the horizontal wavenumber are calculated for horizontal planes located at given heights at fixed points in time. On such a plane, values of the simulated hydrodynamic variable f_i are set in the nodes of the horizontal grid with coordinates x_i, i=1, 2, ..., N. For any k_h=k_x, these values can be approximated by the sum of the cosine and sine Fourier transforms

$$f_c = X\left(k_h\right)\cos\left(k_h x\right) + Y\left(k_h\right)\sin\left(k_h x\right). \qquad (2)$$

After determining $X(k_h)$ and $Y(k_h)$ by the least square method, the amplitude $A_f(k_h)$ and the spectral density $S_f(k_h)$ are calculated using formulas

$$A_f\left(k_h\right) = \sqrt{X^2 + Y^2},\ S_f\left(k_h\right) = \frac{L_h A_f^2}{2\pi}. \qquad (3)$$

The calculations are equivalent to the widespread Lomb—Scargle spectral analysis method [Lomb, 1976; Scargle, 1982]. For equally spaced grid nodes x_i, applying (2), (3) yields the same results as the fast Fourier transform, yet procedures (2), (3) are also applicable to the grids with unequally spaced nodes.

The left plot of Figure 1 shows the spatial spectral density $S_w(k_h)$ of vertical velocity at an altitude of 0.1 km near the wave source at the lower boundary of the atmosphere for t=t_a+40 hr. The spectrum in the left plot is dominated by the spectral component with k_{h1}=2π/λ_{h1} corresponding to the primary AGW with a horizontal length λ_{h1}=840 km, which is generated by surface wave source (1). In addition, the spectrum in the left plot has a continuum formed by secondary AGWs and mathematical errors arising in the numerical model.

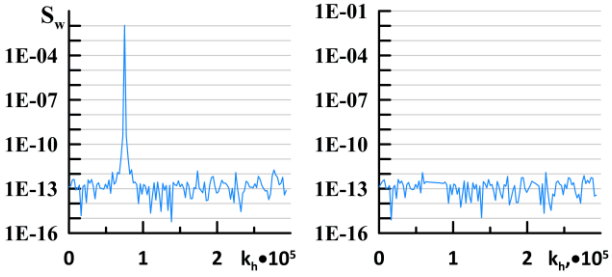

Figure 1. Spectral density of model variations in vertical velocity (in m^3/s^2) as function of k_h (m^{-1}) on a horizontal plane located at an altitude of 0.1 km for t=t_a+40 hr (left) and the result of exclusion of primary AGW (right) for wave source (1) on the Earth surface with W_0=0.1 mm/s and a horizontal phase velocity c_h=100 m/s

The primary AGW has the form of a plane wave of the same amplitude on the entire horizontal plane, which allows us to distinguish between the spectra of primary and secondary AGWs. The presence of nonuniformity of the horizontal velocity in the numerical model can lead to local changes in the horizontal wavenumber. Therefore, the peak corresponding to the primary AGW in the left plot is widened and occupies a certain range of wave numbers $k_h \in [k_{h1}-\varepsilon, k_{h1}+\varepsilon]$ near the main maximum at $k_h=k_{h1}$. The right plot displays the spectral density $S'_f(k_h)$ after exclusion of spectral components in the ε-neighborhood of the main maximum. In this region, the spectrum in the right plot of in the range $k_h \in [k_{h1}-\varepsilon, k_{h1}+\varepsilon]$ is changed for linear interpolation between values at the boundaries of the range.

Such spectra separation makes it possible to determine the variances of f variations induced by primary (δ^2_{f1}) and secondary (δ^2_{f2}) AGW modes:

$$\delta^2_{f1} = \int_{k_{h1}-\varepsilon}^{k_{h1}+\varepsilon} S_f(k_h)\,dk_h,$$
$$\delta^2_{f2} \int_{k_{h0}}^{k_{hm}} S'_f(k_h)\,dk_h, \qquad (4)$$

where k_{h0} and k_{hm} are minimum and maximum boundary values of the spectral region we analyze.

The spectrum in the right plot contains information about secondary AGWs occurring during evolution and interactions of a primary wave generated in the model with a surface wave source. This open up new opportunities for studying the occurrence of secondary waves under various atmospheric conditions.

3. EVOLUTION OF THE SPECTRUM OF SECONDARY AGWs

Figure 1 demonstrates that at a very low height in the immediate vicinity of the source, the primary wave dominates, so it would be well to examine similar spectra at other heights and at other time points. Figure 2 illustrates the spectra of model variations in vertical velocity at different heights in the middle and upper atmosphere. It is apparent that in the mesosphere and thermosphere in the spectra, along with the main peak of primary AGW with $k_h=k_{h1}$ there are peaks at multiples of wave numbers $k_{h2}=2\,k_{h1}$ and $k_{h3}=3\,k_{h1}$. These peaks are peculiar to secondary wave modes, which arise due to the nonlinearity of hydrodynamic equations.

Table 1 lists the amplitudes peculiar to the spectral peaks of primary and secondary AGW modes shown in Figure 2. The amplitude of primary AGW is seen to peak at ~100 km and decrease somewhat at higher altitudes. This can be explained by the increase in molecular viscosity and thermal conductivity at higher altitudes, as well as by the transition of part of the wave energy from AGW to the mean flow induced by waves above 100 km (see [Gavrilov et al., 2022]).

Figure 3 and Table 1 suggest that at 150–200 km W_1 is higher for a wave with c_h=100 m/s as compared to the AG`W having c_h=50 m/s. According to the dispersion equation of the theory of atmospheric AGWs, a faster wave has a longer vertical length and undergoes weaker

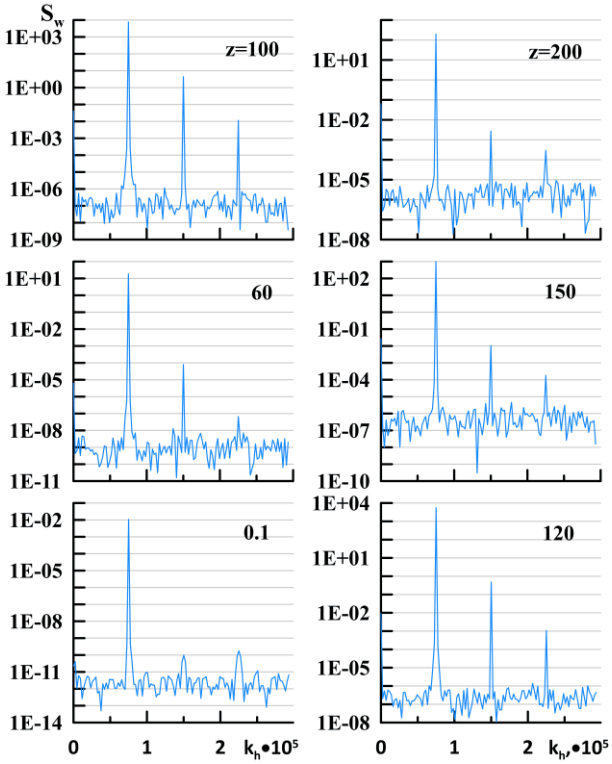

Figure 2. Spectral density of model variations in vertical velocity (in m^3/s^2) as function of k_h (in m^{-1}) on horizontal planes located at different heights (marked with numbers in km) at $t=t_a$+40 hr for wave source (1) on the Earth surface with W_0=0.1 mm/s and a horizontal phase velocity c_h=50 m/s

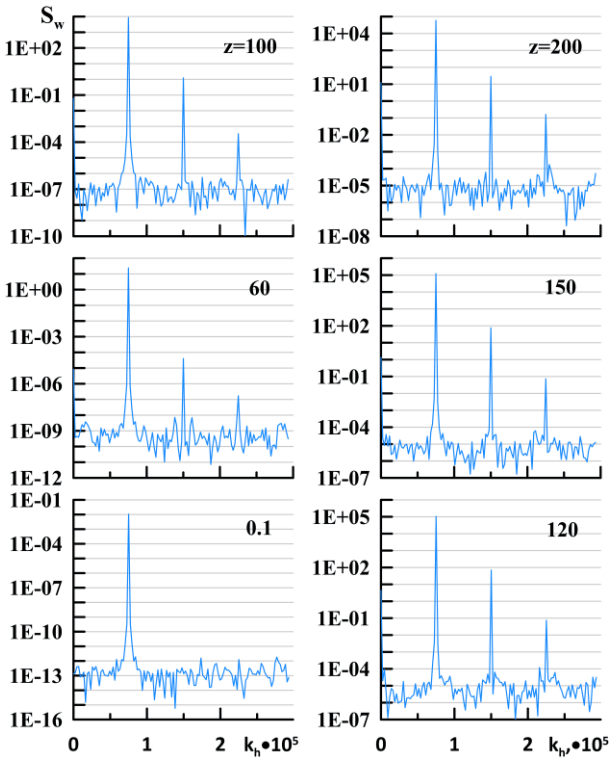

Figure 3. The same as in Figure 2 for a wave source with c_h=100 m/s

Table 1

Amplitude of primary AGW W_1 (the main spectral peak in Figure 2) and relative amplitudes of secondary waves W_2, W_3 corresponding to two subsequent spectral peaks at $t = t_a$+40 hr

z, km	c_h=50 m/s			c_h=100 m/s		
	W_1, mm/s	W_2/W_1, %	W_3/W_1, %	W_1, mm/s	W_2/W_1, %	W_3/W_1, %
0.1	0.10	0.009	0.013	0.10	0.001	0.001
60	4.18	0.206	0.006	4.76	0.129	0.008
100	84.8	2.404	0.123	90.2	1.200	0.020
120	72.4	0.929	0.044	31.4	2.574	0.085
150	30.6	0.327	0.043	34.0	2.499	0.077
200	13.7	0.372	0.121	23.6	2.202	0.165

dissipation in the upper atmosphere. Figures 2 and 3 refer to a fixed moment of the model time after activation of surface AGW source (1).

The time evolution of wave spectra at z=100 km is illustrated in Figure 4, and the corresponding amplitudes of primary and secondary AGWs are shown in Table 2. Table 1 indicates that in the numerical experiment $W_2/W_1 \approx \delta_{w2}/\delta_{w1} \sim 2.5$ % at 120–150 km for AGW with c_h=100 m/s. In Table 1, for a slower mode with c_h=50 m/s, the ratios $(W_2/W_1)_{50}$ and $(W_3/W_1)_{50}$ exceed $(W_2/W_1)_{100}$ and $(W_3/W_1)_{100}$ for a wave with c_h=100 m/s at 100 km, whereas at high altitudes $(W_2/W_1)_{50} < (W_2/W_1)_{100}$ and $(W_3/W_1)_{50} < (W_3/W_1)_{100}$. This appears to be due to the shorter vertical length of the slower AGW, which leads to a stronger instability and nonlinearity of the mode with

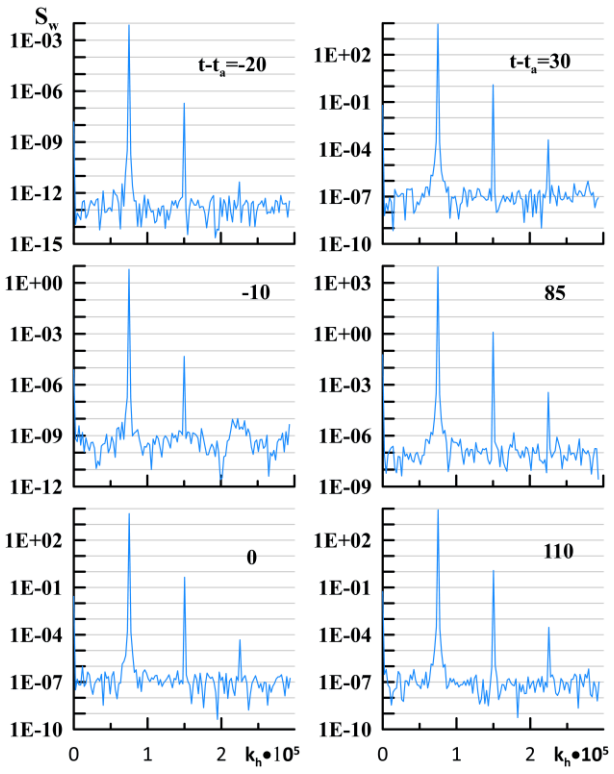

Figure 4. Spectral density of model variations in vertical velocity (in m^3/s^2) as function of k_h (in m^{-1}) on the horizontal plane z=100 km at various moments of model time t–t_a (indicated by numbers in hours) for wave source (1) on the Earth surface with W_0=0.1 mm/s and c_h=100 m/s

Table 2

The same as in Table 1 for 100 km and different time values t–t_a

t–t_a, hr	c_h=100 m/s		
	W_1, mm/s	W_2/W_1, %	W_3/W_1, %
–20	0.09	0.497	0.002
–10	2.44	0.272	0.002
0	67.5	0.958	0.010
30	90.2	1.197	0.021
55	89.6	1.201	0.020
80	88.4	1.199	0.019

c_h=50 m/s near 100 km and to a stronger attenuation of this wave at higher altitudes under the action of molecular viscosity and thermal conductivity.

The small values of W_2/W_1 and W_3/W_1 in Tables 1 and 2 suggest that in the cases we analyze the amplitudes and momentum and energy fluxes of secondary waves are lower than those of the primary AGW. This is due to the relatively weak nonlinear interactions during propagation of low-amplitude AGWs in the background temperature and wind fields, which do not contain convective and shear instabilities and critical levels. With an increase in the amplitude of wave sources and in the presence of instabilities and critical levels, the relative percentage of secondary AGWs may increase. Moreover, components with large vertical wavelengths may appear in the spectrum of secondary AGWs, which are subject to weaker dissipation and can more easily penetrate into the upper atmosphere. Studying these processes requires further simulation and observation of secondary AGWs in the atmosphere.

CONCLUSION

We have simulated plane AGWs in the high-resolution nonlinear model AtmoSym and have separated spectra of primary waves, generated by a wave source at the lower boundary of the model, and secondary modes, generated by these primary waves at different heights of the middle and upper atmosphere. Examples are given which illustrate the gradual formation of the spectrum of secondary waves after switching on the wave source in the model. It is shown that a short time after switching on the plane wave source at the lower

boundary of the model, the spectrum consists of a peak corresponding to primary AGW and white noise generated by random atmospheric disturbances and noise of the numerical model. Later on, peaks of secondary wave modes with horizontal wave numbers that are multiples of the wave numbers of primary AGW appear in the spectra. Separating the spectra of primary and secondary AGWs allows us to estimate the relative contribution of secondary AGWs at different altitudes, at different times, and with different stability of the background temperature and wind profiles in the atmosphere.

Because of the limited computational power, in this paper we have performed simulation with a sufficiently large step of the horizontal grid and have analyzed only the primary wave and the first two spectral peaks of secondary modes. A similar simulation with a smaller step is required to examine the features of the formation of the secondary AGW spectrum in a wider range of wave numbers. Further simulation is also required to study the relative contribution of secondary AGWs to the wave momentum and energy flows with increasing amplitude of wave sources and in the presence of instabilities and critical levels created by background temperature and wind fields.

The work was financially supported by the Russian Science Foundation (Grant No. 22-27-00171).

REFERENCES

Alexander M.J., Geller M., McLandress C., Polavarapu S., Preusse P., Sassi F.,Sato K., Eckermann S., Ern M., Hertzog A., et al. Recent developments in gravity-wave effects in climate models and the global distribution of gravity-wave momentum flux from observations and models. *Quarterly Journal of the Royal Meteorological Society. Part A*. 2010, vol. 136, iss. 650, pp. 1103–1124. DOI: 10.1002/qj.637.

Azeem I., Vadas S.L., Crowley G., Makela J.J. Traveling ionospheric disturbances over the United States induced by gravity waves from the 2011 Tohoku tsunami and comparison with gravity wave dissipative theory. *J. Geophys. Res.: Space Phys.* 2017, vol. 122, iss. 3, pp. 3430–3447. DOI: 10.1002/2016JA023659.

Bacmeister J.T., Schoeberl M.R. Breakdown of vertically propagating two-dimensional gravity waves forced by orography. *J. Atmos. Sci*. 1989, vol. 46, pp. 2109–2134.

Becker E., Knopfel R., Lubken F.-J. Dynamically induced hemispheric differences in the seasonal cycle of the summer polar mesopause. *J. Atmos. Solar-Terr. Phys*. 2015, vol. 129, pp. 128–141. DOI: 10.1016/j.jastp.2015.04.014.

Chen C., Chu X., Zhao J., Roberts B.R., Yu Z., Fong W., Lu X., Smith J.A. Lidar observations of persistent gravity waves with periods of 3–10 h in the Antarctic middle and upper atmosphere at McMurdo (77.83° S, 166.67° E). *J. Geophys. Res:. Space Phys*. 2016, vol. 121, pp. 1483–1502. DOI: 10.1002/2015JA022127.

Franke P.M., Robinson W.A. Nonlinear behavior in the propagation of atmospheric gravity waves. *J. Atmos. Sci*. 1999, vol. 56, pp. 3010–3027.

Fritts D.C., Vadas S.L., Wan K., Werne J.A. Mean and variable forcing of the middle atmosphere by gravity waves. *J. Atmos. Solar-Terr. Phys*. 2006, vol. 68, no. 3-5, pp. 247–265. DOI: 10.1016/j.jastp.2005.04.010.

Fritts D.C., Wang L., Werne J. Gravity wave–fine structure interactions: A reservoir of small-scale and large-scale turbulence energy. *Geophys. Res. Lett*. 2009, vol. 36, no. 19, L19805. DOI: 10.1029/2009GL039501.

Fritts D.C., Wan K., Werne J., Lund T., Hecht J.H. Modeling the implications of Kelvin-Helmholtz instability dynamics for airglow observations. *J. Geophys. Res.: Atmos*. 2014, vol. 119, pp. 8858–8871. DOI: 10.1002/2014JD021737.

Gassmann A., Herzog H.-J. How is local material entropy production represented in a numerical model? *Quarterly Journal of the Royal Meteorological Society*. 2015, vol. 141, pp. 854–869. DOI: 10.1002/qj.2404.

Gavrilov N.M., Kshevetskii S.P., Numerical modeling of the propagation of nonlinear acoustic-gravity waves in the middle and upper atmosphere. *Izvestiya. Atmos. Oceanic Phys*. 2014, vol. 50, no. 1, pp. 66–72. DOI: 10.1134/S0001433813050046.

Gavrilov N.M., Kshevetskii S.P., Koval A.V. Verifications of the high-resolution numerical model and polarization relations of atmospheric acoustic-gravity waves. *Geoscientific Model Development*. 2015, vol. 8, pp. 1831–1838. DOI: 10.5194/gmd-8-1831-2015.

Gavrilov N.M., Kshevetskii S.P., Koval A.V. Decay times of atmospheric acoustic–gravity waves after deactivation of wave forcing. *Atmos. Chem. Phys*. 2022, vol. 22, pp. 3713–3724. DOI: 10.5194/acp-22-13713-2022.

Geller M.A., Alexander M.J., Love P.T., Bacmeister J., Ern M., Hertzog A., Manzini E., Preusse P., Sato K., Scaife A.A., Zhou T. A comparison between gravity wave momentum fluxes in observations and climate models. *J. Climate*. 2013, vol. 26, iss. 17, pp. 6383–6405. DOI: 10.1175/JCLI-D-12-00545.1.

Gossard E.E., Hooke W.H. *Waves in the Atmosphere: Atmospheric Infrasound and Gravity Waves: Their Generation and Propagation*. Elsevier Sci. Publ. Co., (Developments in Atmosph. Sci., no. 2) 1975. 470 p.

Kikoin I.K. *Tables of Physical Quantities.* Moscow, Atomizdat Publ., 1976, pp. 272–279.

Liu X., Xu J., Liu H., Ma R. Nonlinear interactions between gravity waves with different wavelengths and diurnal tide. *J. Geophys. Res.: Atmos*. 2008, vol. 1139, no. 8, D08112. DOI: 10.1029/2007JD009136.

Lomb N. Least-squares frequency analysis of unequally spaced data. *Astrophys. Space Sci*. 1976, vol. 39, no. 2, pp. 447–462.

Miyoshi Y., Fujiwara H. Gravity waves in the thermosphere simulated by a general circulation model. *J. Geophys. Res*.: *Atmos.* 2008, vol. 113, no. 1, D01101. DOI: 10.1029/2007JD008874.

Miyoshi Y., Fujiwara H., Jin H., Shinagawa H. A global view of gravity waves in the thermosphere simulated by a general circulation model. *J. Geophys. Res.: Space Phys*. 2014, vol. 119, iss. 7, pp. 5807–5820. DOI: 10.1002/2014JA019848.

Picone J.M., Hedin A.E., Drob D.P., Aikin A.C. NRLMSISE-00 empirical model of the atmosphere: Statistical comparisons and scientific issues. *J. Geophys. Res*. 2002, vol. 107, iss. A12, 1468. DOI: 10.1029/2002JA009430.

Scargle J.D. Statistical aspects of spectral analysis of unevenly spaced data. *Astrophys. J. Part 1*. 1982, vol. 263, pp. 835–853.

Smith R.B., Nugent A.D., Kruse C.G., Fritts D., Doyle J.D., Eckermann S.D., Taylor M.J., Dörnbrack A., Uddstrom M., Cooper W., Romashkin P., Jensen J., Beaton S. Stratospheric gravity wave fluxes and scales during DEEPWAVE. *J. Atmos. Sci*. 2016, vol. 73, iss. 7, pp. 2581–2869. DOI: 10.1175/JAS-D-15-0324.1.

Townsend A.A. Excitation of internal waves by a turbulent boundary layer. *Journal of Fluid Mechanics*. 1965, vol. 22, pp. 241–252.

Townsend A.A. Internal waves produced by a convective layer. *Journal of Fluid Mechanics*. 1966, vol. 24, pp. 307–319.

Vadas S.L., Fritts D.C. The importance of spatial variability in the generation of secondary gravity waves from local body forces. *Geophys. Res. Lett*. 2002, vol. 29, no. 20, 1984. DOI: 10.1029/2002GL015574.

Vadas S.L., Crowley G. Sources of the traveling ionospheric disturbances observed by the ionospheric TIDDBIT sounder near Wallops Island on 30 October 2007. *J. Geophys. Res*. 2010, vol. 115, A07324. DOI: 10.1029/2009JA015053.

Vadas S.L., Crowley G. Neutral wind and density perturbations in the thermosphere created by gravity waves observed by the TIDDBIT sounder. *J. Geophys. Res.: Space Phys*. 2017, vol. 122, pp. 6652–6678. DOI: 10.1002/2016JA023828.

Vadas S.L., Liu H.-L. Numerical modeling of the large-scale neutral and plasma responses to the body forces created by the dissipation of gravity waves from 6 h of deep convection in Brazil. *J. Geophys. Res.: Space Phys*. 2013, vol. 118, pp. 2593–2617. DOI: 10.1002/jgra.50249.

Yiğit E., Medvedev A.S. Heating and cooling of the thermosphere by internal gravity waves. *Geophys. Res. Lett*. 2009, vol. 36, L14807. DOI: 10.1029/2009GL038507.

Yiğit E., Medvedev A.S., Aylward A.D., Hartogh P., Harris M.J. Modeling the effects of gravity wave momentum deposition on the general circulation above the turbopause. *J. Geophys. Res*. 2009, vol. 114, iss. D7, D07101. DOI: 10.1029/2008JD011132.

Yu Y., Hickey M.P., Liu Y. A numerical model characterising internal gravity wave propagation into the upper atmosphere. *Adv. Space Res*. 2009, vol. 44, pp. 836–846. DOI: 10.1016/j.asr.2009.05.014.

Zhao J., Chu X., Chen C., Lu X., Fong W., Yu Z., Jones R.M., Roberts B.R., Dörnbrack A. Lidar observations of stratospheric gravity waves from 2011 to 2015 at McMurdo (77.84° S, 166.69° E), Antarctica: 1. Vertical wavelengths, periods, and frequency and vertical wave number spectra. *J. Geophys. Res.: Atmos*. 2017, vol. 122, iss. 10, pp. 5041–5062. DOI: 10.1002/2016JD026368.

URL: http://atmos.kantiana.ru/language/ru (accessed February 15, 2023).

Original Russian version: Gavrilov N.M., Kshevetskii S.P., published in Solnechno-zemnaya fizika. 2023. Vol. 9. Iss. 3. P. 93–99. DOI: 10.12737/szf-93202310.

How to cite this article

Gavrilov N.M., Kshevetskii S.P. Identification of spectrum of secondary acoustic-gravity waves in the middle and upper atmosphere in a high-resolution numerical model. *Solar-Terrestrial Physics*. 2023. Vol. 9. Iss. 3. P. 86–92. DOI: 10.12737/stp-93202310.